COMPUTER RESEARCH AND MODELING
2026 VOL. 18 NO. 4 P. 973–988
DOI: 10.20537/2076-7633-2026-18-4-973-988

UDC: 004.942

Finite element algorithm for lumbar spine modeling incorporating physical nonlinearity of material

K. S. Kurochka[1,a], V. V. Komrakov[1,b], E. L. Tsitko[2,c], K. A. Panarin[1,d], T. S. Semenchenya[1,e]

[1]Gomel State Technical University named after P. O. Sukhoi,
48 prospekt Oktyabrya, Gomel, 246029, Belarus
[2]Gomel regional clinical hospital,
5 Brat'ev Lizyukovykh st., Gomel, 246029, Belarus

E-mail: [a] konstantsinkurochka@gmail.com, [b] msf_vdos@mail.ru, [c] fedor30@tut.by, [d] logran2@gmail.com, [e] levts@gstu.by

Received 19.02.2026, after completion — 08.05.2026.
Accepted for publication 05.07.2026.

This paper presents the development and verification of a finite element algorithm for modeling nonlinear deformation in the functional spinal unit (FSU) of the human lumbar spine. The study is motivated by the increasing prevalence of musculoskeletal disorders and the need for improved predictive methods for spinal motion segment behavior under various loading conditions and pathologies.

Current modeling approaches often employ simplified geometry and linear deformation laws (Hooke's law) for all spinal elements, including the intervertebral disc. However, these models inadequately represent human anatomy and the physical properties of the intervertebral disc, which comprises the annulus fibrosus and nucleus pulposus exhibiting pronounced nonlinear and viscoelastic characteristics.

To address these limitations, the authors propose a mathematical model wherein vertebrae are treated as linearly elastic, heterogeneous bodies, while the intervertebral disc is modeled according to nonlinear deformation theory. An anatomically accurate 3D reconstruction of the lumbar spine was generated from computed tomography (CT) images. Volumetric tetrahedral finite elements were employed for discretization. The intervertebral disc behavior is described using thin plate bending theory based on Kirchhoff-Love assumptions.

The algorithm's key feature is a two-step solution procedure: an initial linear elastic solution is obtained, followed by the calculation of additional nodal forces for disc elements, enabling efficient nonlinear analysis without stiffness matrix modification.

Model verification was performed using two geometric representations of the lumbar spine: a simplified version comprising parallelepipeds and cylinders, and a patient-specific realistic model derived from CT data. Numerical simulation results demonstrate that incorporating nonlinear properties of the intervertebral disc substantially alters both deformation patterns and magnitudes compared to purely elastic models, producing nonlinear segments on stress-strain curves. The discrepancy between results obtained with the proposed algorithm and those from Comsol software did not exceed 10 %, confirming the model's validity. This algorithm shows promise for investigating lumbar spine biomechanics under normal conditions, degenerative changes, and post-surgical states.

Keywords: finite element method, convergence, lumbar spine, vertebrae, intervertebral disc

Citation: *Computer Research and Modeling*, 2026, vol. 18, no. 4, pp. 973–988.

**КОМПЬЮТЕРНЫЕ ИССЛЕДОВАНИЯ
И МОДЕЛИРОВАНИЕ 2026 Т. 18 № 4 С. 973–988**
DOI: 10.20537/2076-7633-2026-18-4-973-988

УДК: 004.942

Алгоритм конечных элементов для моделирования поясничного отдела позвоночника с учетом физической нелинейности материала

К. С. Курочка[1,a], В. В. Комраков[1,b], Е. Л. Цитко[2,c], К. А. Панарин[1,d], Т. С. Семенченя[1,e]

[1]Гомельский государственный технический университет имени П. О. Сухого,
Беларусь, 246029, г. Гомель, проспект Октября, д. 48
[2]Гомельская областная клиническая больница,
Беларусь, 246029, г. Гомель, ул. Братьев Лизюковых, д. 5

E-mail: [a] konstantsinkurochka@gmail.com, [b] msf_vdos@mail.ru, [c] fedor30@tut.by, [d] logran2@gmail.com, [e] levts@gstu.by

Получено 19.02.2026, после доработки — 08.05.2026.
Принято к публикации 05.07.2026.

В данной статье представлены разработка и верификация алгоритма конечных элементов для моделирования нелинейной деформации в позвоночно-двигательном сегменте (ПДС) поясничного отдела позвоночника человека. Исследование мотивировано растущей распространенностью заболеваний опорно-двигательного аппарата и необходимостью улучшения методов прогнозирования поведения сегментов позвоночника при различных условиях нагрузки и патологиях.

Современные подходы к моделированию часто используют упрощенную геометрию и линейные законы деформации (закон Гука) для всех элементов позвоночника, включая межпозвоночный диск. Однако эти модели неадекватно представляют анатомию человека и физические свойства межпозвоночного диска, который состоит из фиброзного кольца и пульпозного ядра, демонстрирующих выраженные нелинейные и вязкоупругие характеристики.

Для решения этих проблем авторы предлагают математическую модель, в которой позвонки рассматриваются как линейно упругие, неоднородные тела, а межпозвоночный диск моделируется в соответствии с теорией нелинейной деформации. Анатомически точная 3D-реконструкция поясничного отдела позвоночника была создана на основе изображений компьютерной томографии (КТ). Для дискретизации использовались объемные тетраэдрические конечные элементы. Поведение межпозвоночного диска описывается с помощью теории изгиба тонких пластин, основанной на предположениях Кирхгофа – Лава.

Ключевой особенностью алгоритма является двухэтапная процедура решения: сначала получается линейно-упругое решение, а затем вычисляются дополнительные узловые силы для элементов диска, что позволяет проводить эффективный нелинейный анализ без модификации матрицы жесткости.

Проверка модели проводилась с использованием двух геометрических представлений поясничного отдела позвоночника: упрощенной версии, включающей параллелепипеды и цилиндры, и персонализированной модели, полученной из КТ изображений конкретного пациента. Результаты численного моделирования показывают, что учет нелинейных свойств межпозвоночного диска существенно изменяет как характер, так и величину деформаций по сравнению с чисто упругими моделями, создавая нелинейные сегменты на кривых «напряжение – деформация». Расхождение между результатами, полученными с помощью предложенного алгоритма, и результатами, полученными с помощью программного обеспечения Comsol, не превышало 10 %, что подтверждает достоверность модели. Данный алгоритм демонстрирует перспективность для исследования биомеханики поясничного отдела позвоночника в нормальных условиях, при дегенеративных изменениях и послеоперационном периоде.

Ключевые слова: метод конечных элементов, сходимость, поясничный отдел позвоночника, позвонки, межпозвоночный диск

Introduction

Rising urbanization, environmental factors, and global population aging have contributed to a growing prevalence of musculoskeletal disorders (MSDs), particularly affecting large joints and the spine. Modern diagnostic technologies have significantly expanded opportunities for in vivo assessment of physiological and pathological spinal conditions [Korzh et al., 2015; Yang et al., 2016]. Clinicians primarily rely on clinical examinations and imaging modalities (X-ray, CT, or magnetic resonance imaging (MRI)) to determine treatment strategies. However, these tools provide only static morphological data, capturing structural changes in the spine and paravertebral tissues at various stages of degenerative disc disease or treatment. Such information is insufficient for predicting disease progression or complication risks. Furthermore, standard imaging cannot quantify the mechanical properties of pathological spinal motion segments (SMS) or their impact on spinal kinematics. Biomechanical studies are therefore essential to:

- evaluate spinal behavior under physiological, loaded, and pathological conditions;
- guide mechanism-based treatment selection;
- develop novel corrective, rehabilitative, and functional assessment strategies [Korzh et al., 2015; Yang et al., 2016].

One established computational approach employs simplified geometries and material models for spinal components. These models typically use idealized shapes with averaged dimensions for vertebrae and intervertebral discs [Ablyazov et al., 2014; Tsurova, 2011; Korzh et al., 2012; Bublik, Likholetov, 2014; Mezentsev et al., 2011; Orlov, 2011; Veretelnik et al., 2014]. Another strategy involves manually measuring key anatomical parameters from medical images and replicating uniform vertebral and disc geometries across a spinal region [Eremin et al., 2011; Bublik et al., 2013; Palatinskaya et al., 2012; Staude et al., 2012]. While this method streamlines 3D model generation and is suitable for healthy spines, it fails to capture degenerative changes that substantially alter vertebral and disc morphology.

Subsequent numerical analyses of the stress – strain distribution (SSD) are typically conducted using static finite element method (FEM) simulations. These studies generally assume small deformations and model all spinal tissues as linearly elastic (Hooke's law) [Ablyazov et al., 2014; Eremin et al., 2011; Korzh et al., 2012; Bublik, Likholetov, 2014; Palatinskaya et al., 2012; Orlov, 2011; Staude et al., 2012]. Consequently, both the mathematical formulations and resulting simulations are highly simplified. More complex models have been developed to simulate surgical interventions, such as external fixation or vertebral body replacement [Tsurova, 2011; Korzh et al., 2012; Bublik, Likholetov, 2014; Bublik et al., 2013; Orlov, 2011]. While metallic implants are appropriately modeled using linear elasticity, the assumption of linear material behavior is often incorrectly extended to biological spinal tissues.

However, numerous studies emphasize that intervertebral disc mechanics deviate significantly from linear elastic assumptions. This is due to the disc's composite structure: the annulus fibrosus, which exhibits pronounced nonlinear and viscoelastic behavior [Barysh et al., 2012; Obraztsov, 1988; Best et al., 1999], and the nucleus pulposus, a gel-like, fluid-rich core [Chou et al., 2006]. Disc nutrition and waste removal are mechanically driven processes that occur during spinal motion (e. g., flexion – extension), where cyclic loading induces pressure gradients that facilitate nutrient influx and metabolite clearance [Zharnov, Zharnova, 2014; Furlong, Palazotto, 1983]. In computational models, the disc is typically represented as a viscoelastic structure sandwiched between adjacent vertebrae.

Nonlinear constitutive relationships for intervertebral disc deformation under static loading have been implemented in finite element analyses of the lumbar spine [Zander et al., 2001]. In the numerical analysis of degenerative changes, reductions in nucleus pulposus volume and altered nonlinear properties of the annulus fibrosus have been explicitly modeled [Cansel, 2018]. Disc prolapse has also been investigated by simulating the nonlinear mechanical response of the annulus fibrosus [Nagy, Gentle, 2001]. Following discectomy, nucleotomy implant models have historically relied on linear-elastic formulations [Meakin, 2001; Joshi et al., 2009]; however, recent silicone-based implants necessitate nonlinear material descriptions [Strange et al., 2010].

Currently, spinal biomechanical models are widely applied to:

- analyze SMS kinematics under physiological and pathological loading;
- objectively assess surgical indications and personalize the extent of intervention;
- predict disease progression and complication risks;
- develop patient-specific rehabilitation protocols.

The aim of this study is to develop a computationally efficient finite element framework for simulating the stress – strain behavior of the lumbar spine, with potential applications in musculoskeletal disorder research. To this end, vertebrae are modeled as linearly elastic heterogeneous bodies, while intervertebral discs are described using a nonlinear constitutive law.

Investigating the biomechanical function of spinal joints under physiological and pathological conditions remains a highly active and promising research area. A robust understanding of spinal mechanics and its disease-induced alterations provides the foundation for next-generation diagnostic and therapeutic technologies.

1. Problem statement and adopted hypotheses

The construction of a mathematical model of the examined system will be based on the systems approach, according to which it is assumed that the system can have a structural representation, i. e., it can be broken down into groups of elements with the indication of connections between them. This splitting is called decomposition, and is preserved for the whole duration of the system. These groups of elements are called modules, in this regard, it is common to talk about the modular structure of the system. The formation of modules is based on the principle of shared properties, the type of connections or other features. This system is complex and consists of different elements. To analyze it, the system approach based on the FEM will be used [Strange et al., 2010].

For this system, we use a micro-level decomposition approach and identify two representative elements: a vertebra and an intervertebral disc. These representative elements share the same structure of inputs, outputs, and external actions. These typical elements will have the same structure of input, output parameters and external influences. In the system under consideration FSU, the acting vertical load determined by the anthropometric parameters of the person under study and the boundary conditions will be the external influences, and the displacements of the elements will be the input and output parameters.

In modeling a vertebra, only its body without processes and connecting arches is taken into account. In this case, the vertebral body has a shape close to a cylinder. We obtained a 3D model of the vertebral body based on CT images of the patient’s spine [Kurachka, Tsalka, 2017]. The space between the vertebrae is filled with another 3D model — a model of the intervertebral disc.

The spatial system under consideration consists of two vertebrae with heterogeneous properties and a nonlinear elastic intervertebral disc located between them (Fig. 1).

The vertebra has a heterogeneous structure. It is covered by a hard cortical layer, spongy bone is located inside the vertebra, and the vertebra is bounded from above and below by hyaline plates covered by articular cartilage (Fig. 1).

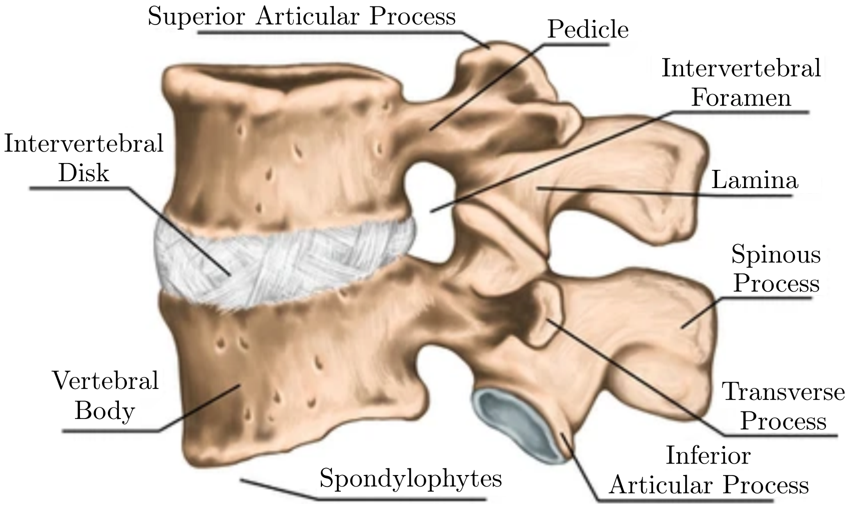

Figure 1. “Vertebra – intervertebral disc – vertebra” system

The intervertebral disc also has a heterogeneous structure [Ablyazov et al., 2014]. The central part is the jelly core (nucleus pulposus), which is surrounded by a shell of collagen fibers — the annulus fibrosus. Until the age of 20 years the nucleus pulposus in humans is well expressed, and then, with age, it is replaced by fibrous connective tissue, sprouting from the annulus fibrosus.

Thus, with age, spinal tissues undergo significant changes in structure and mechanical properties, which are individual, nonlinear, and difficult to predict. In [Anisimova et al., 2015], the authors study interpatient variability (including age-related differences). It is shown that, despite simplifications, the model adequately captures the main biomechanical trends, while interpatient variability increases with progression of “resections”. Therefore, this study uses averaged values of the mechanical characteristics of the intervertebral disc and vertebra for an adult, as presented in Table 1.

Table 1. Mechanical characteristics of spine elements

Spine element	Young’s modulus, Pa	Poisson’s ratio	Density, kg/m^3
Vertebra	$18\,350 \cdot 10^6$	0.3	2020
Intervertebral disc	$57 \cdot 10^6$	0.4	1090.3

The intervertebral disc is fused to the hyaline cartilage covering the surfaces of the vertebral bodies facing each other, and is shaped like these surfaces. Therefore, when combining 3D models of the vertebra and intervertebral disc into one system, their boundaries will be common with the same values of elastic body deformations.

Then, by the principle of virtual displacements [Strange et al., 2010; Coogan et al., 2016], the total potential energy of the system is written as follows:

$$\{\widetilde{\mathbf{g}}\}^{\mathrm{T}}\{\mathbf{R}\} = \iiint\limits_V \{\widetilde{\varepsilon}\}^{\mathrm{T}}\{\sigma\}\, dV, \tag{1}$$

where $\{\mathbf{g}\}$ is the vector of nodal displacements (symbol “~” denotes its variation), $\{\mathbf{R}\}$ is the vector of nodal forces; $\{\varepsilon\}$ is the deformation vector, $\{\sigma\}$ is the stress vector and V is the volume of the finite element.

The vertebrae will be treated as linearly elastic heterogeneous bodies.

The intervertebral disc is nonlinearly elastic and does not change its volume under small loads, so the hypothesis of nonlinear deformations is valid for it [Strange et al., 2010]. According to the decomposition principle, elements will be considered separately.

2. Vertebral finite element model

For discretization we use finite elements in the form of tetrahedrons [Goto et al., 2007]. Nodal forces are applied to the vertices of each tetrahedron

$$\left\{\mathbf{R}^{\mathrm{V}}\right\}^{\mathrm{T}} = \{X_1, Y_1, Z_1, X_2, Y_2, Z_2, X_3, Y_3, Z_3, X_4, Y_4, Z_4\},$$

to which the following nodal displacements would correspond:

$$\left\{\mathbf{g}^{\mathrm{V}}\right\}^{\mathrm{T}} = \{u_1, \vartheta_1, w_1, u_2, \vartheta_2, w_2, u_3, \vartheta_3, w_3, u_4, \vartheta_4, w_4\},$$

where u, ϑ, w are movements along the OX, OY, and OZ axes. For the tetrahedron it is possible to take linear functions for the displacements [Goto et al., 2007]:

$$\begin{gathered} u = \alpha_1 + \alpha_2 x + \alpha_3 y + \alpha_4 z, \\ \vartheta = \alpha_5 + \alpha_6 x + \alpha_7 y + \alpha_8 z, \\ w = \alpha_9 + \alpha_{10} x + \alpha_{11} y + \alpha_{12} z \end{gathered} \tag{2}$$

or

$$\left\{\mathbf{g}_0^{\mathrm{V}}\right\} = \left[\mathbf{A}^{\mathrm{V}}\right]\left\{\alpha^{\mathrm{V}}\right\},$$

where

$$\left[\mathbf{A}^{\mathrm{V}}\right] = \begin{bmatrix} 1 & x & y & z & 0 & 0 & 0 & 0 & 0 & 0 & 0 & 0 \\ 0 & 0 & 0 & 0 & 1 & x & y & z & 0 & 0 & 0 & 0 \\ 0 & 0 & 0 & 0 & 0 & 0 & 0 & 0 & 1 & x & y & z \end{bmatrix}, \quad \left\{\alpha^{\mathrm{V}}\right\}^{\mathrm{T}} = \left\{\alpha_1 \quad \alpha_2 \quad \cdots \quad \alpha_{12}\right\}.$$

Since expression (2) applies to any point of the tetrahedron, for its nodes it follows that

$$\left\{\mathbf{g}^{\mathrm{V}}\right\} = \left[\mathbf{B}^{\mathrm{V}}\right]\left\{\boldsymbol{a}^{\mathrm{V}}\right\}, \tag{3}$$

where

$$\left[\mathbf{B}^{\mathrm{V}}\right] = \begin{bmatrix} 1 & x_1 & y_1 & z_1 & 0 & 0 & 0 & 0 & 0 & 0 & 0 & 0 \\ 0 & 0 & 0 & 0 & 1 & x_1 & y_1 & z_1 & 0 & 0 & 0 & 0 \\ 0 & 0 & 0 & 0 & 0 & 0 & 0 & 0 & 1 & x_1 & y_1 & z_1 \\ 1 & x_2 & y_2 & z_2 & 0 & 0 & 0 & 0 & 0 & 0 & 0 & 0 \\ 0 & 0 & 0 & 0 & 1 & x_2 & y_2 & z_2 & 0 & 0 & 0 & 0 \\ 0 & 0 & 0 & 0 & 0 & 0 & 0 & 0 & 1 & x_2 & y_2 & z_2 \\ 1 & x_3 & y_3 & z_3 & 0 & 0 & 0 & 0 & 0 & 0 & 0 & 0 \\ 0 & 0 & 0 & 0 & 1 & x_3 & y_3 & z_3 & 0 & 0 & 0 & 0 \\ 0 & 0 & 0 & 0 & 0 & 0 & 0 & 0 & 1 & x_3 & y_3 & z_3 \\ 1 & x_4 & y_4 & z_4 & 0 & 0 & 0 & 0 & 0 & 0 & 0 & 0 \\ 0 & 0 & 0 & 0 & 1 & x_4 & y_4 & z_4 & 0 & 0 & 0 & 0 \\ 0 & 0 & 0 & 0 & 0 & 0 & 0 & 0 & 1 & x_4 & y_4 & z_4 \end{bmatrix},$$

x_i, y_i, z_i ($i = \overline{1, 4}$) are the node coordinates of the tetrahedron.

Assuming that the nodal displacement vector is already known $\left\{\mathbf{g}^{\mathrm{V}}\right\}$, we find from (4) the vector of coefficients $\left\{\alpha^{\mathrm{V}}\right\}$:

$$\left\{a^{\mathrm{V}}\right\} = \left[\mathbf{B}^{\mathrm{V}}\right]^{-1}\left\{\boldsymbol{g}^{\mathrm{V}}\right\}, \tag{4}$$

where

$$\left[\mathbf{B}^{\mathrm{V}}\right]^{-1} = \frac{1}{6V}\begin{bmatrix} a_1 & 0 & 0 & a_2 & 0 & 0 & a_3 & 0 & 0 & a_4 & 0 & 0 \\ b_1 & 0 & 0 & b_2 & 0 & 0 & b_3 & 0 & 0 & b_4 & 0 & 0 \\ c_1 & 0 & 0 & c_2 & 0 & 0 & c_3 & 0 & 0 & c_4 & 0 & 0 \\ d_1 & 0 & 0 & d_2 & 0 & 0 & d_3 & 0 & 0 & d_4 & 0 & 0 \\ 0 & a_1 & 0 & 0 & a_2 & 0 & 0 & a_3 & 0 & 0 & a_4 & 0 \\ 0 & b_1 & 0 & 0 & b_2 & 0 & 0 & b_3 & 0 & 0 & b_4 & 0 \\ 0 & c_1 & 0 & 0 & c_2 & 0 & 0 & c_3 & 0 & 0 & c_4 & 0 \\ 0 & d_1 & 0 & 0 & d_2 & 0 & 0 & d_3 & 0 & 0 & d_4 & 0 \\ 0 & 0 & a_1 & 0 & 0 & a_2 & 0 & 0 & a_3 & 0 & 0 & a_4 \\ 0 & 0 & b_1 & 0 & 0 & b_2 & 0 & 0 & b_3 & 0 & 0 & b_4 \\ 0 & 0 & c_1 & 0 & 0 & c_2 & 0 & 0 & c_3 & 0 & 0 & c_4 \\ 0 & 0 & d_1 & 0 & 0 & d_2 & 0 & 0 & d_3 & 0 & 0 & d_4 \end{bmatrix},$$

V is the volume of the elementary tetrahedron,

$$a_i = (-1)^{i+1}\begin{vmatrix} x_j & y_j & z_j \\ x_k & y_k & z_k \\ x_n & y_n & z_n \end{vmatrix}, \quad b_i = (-1)^{i}\begin{vmatrix} 1 & y_j & z_j \\ 1 & y_k & z_k \\ 1 & y_n & z_n \end{vmatrix}, \quad c_i = (-1)^{i+1}\begin{vmatrix} 1 & x_j & z_j \\ 1 & x_k & z_k \\ 1 & x_n & z_n \end{vmatrix}, \quad d_i = (-1)^{i}\begin{vmatrix} 1 & x_j & y_j \\ 1 & x_k & y_k \\ 1 & x_n & y_n \end{vmatrix},$$

i, j, k, n are the vertex numbers of the elementary tetrahedron.

The deformation components are related to the displacements by the Cauchy relations [Goto et al., 2007]:

$$\varepsilon_x = \frac{\partial u}{\partial x}; \quad \varepsilon_y = \frac{\partial \vartheta}{\partial y}; \quad \varepsilon_z = \frac{\partial w}{\partial z}; \quad \gamma_{xy} = \frac{\partial u}{\partial y} + \frac{\partial \vartheta}{\partial x}; \quad \gamma_{yz} = \frac{\partial \vartheta}{\partial z} + \frac{\partial w}{\partial y}; \quad \gamma_{zx} = \frac{\partial u}{\partial z} + \frac{\partial w}{\partial x}. \tag{5}$$

Substituting (3) into (5) and differentiating, we obtain

$$\{\varepsilon\} = \left[\mathbf{C}^{\mathrm{V}}\right]\left\{\alpha^{\mathrm{V}}\right\}, \tag{6}$$

where

$$\left[\mathbf{C}^{\mathrm{V}}\right] = \begin{bmatrix} 0 & 1 & 0 & 0 & 0 & 0 & 0 & 0 & 0 & 0 & 0 & 0 \\ 0 & 0 & 0 & 0 & 0 & 0 & 1 & 0 & 0 & 0 & 0 & 0 \\ 0 & 0 & 0 & 0 & 0 & 0 & 0 & 0 & 0 & 0 & 0 & 1 \\ 0 & 0 & 1 & 0 & 0 & 1 & 0 & 0 & 0 & 0 & 0 & 0 \\ 0 & 0 & 0 & 0 & 0 & 0 & 0 & 1 & 0 & 0 & 1 & 0 \\ 0 & 0 & 0 & 1 & 0 & 0 & 0 & 0 & 0 & 1 & 0 & 0 \end{bmatrix}.$$

For each element of a vertebra according to the accepted hypotheses, Hooke's law is valid [Goto et al., 2007]:

$$\{\sigma\} = [\mathbf{E}_0]\{\varepsilon\}, \tag{7}$$

where

$$[\mathbf{E}_0] = \begin{bmatrix} 2G+\lambda & \lambda & \lambda & 0 & 0 & 0 \\ \lambda & 2G+\lambda & \lambda & 0 & 0 & 0 \\ \lambda & \lambda & 2G+\lambda & 0 & 0 & 0 \\ 0 & 0 & 0 & G & 0 & 0 \\ 0 & 0 & 0 & 0 & G & 0 \\ 0 & 0 & 0 & 0 & 0 & G \end{bmatrix},$$

$\lambda = \frac{\mu E}{(1-2\mu)(1+\mu)}$ is the Lamé parameter (G. Lamé) and $G = \frac{E}{2(1+\mu)}$ is shear modulus.

Substituting equality (4) into (6) and then (6) into (7), respectively, we obtain

$$\{\varepsilon\} = \left[\mathbf{C}^{\mathrm{V}}\right]\left[\mathbf{B}^{\mathrm{V}}\right]^{-1}\left\{\mathbf{g}^{\mathrm{V}}\right\}, \quad \{\sigma\} = \left[\mathbf{E}_0\right]\left[\mathbf{C}^{\mathrm{V}}\right]\left[\mathbf{B}^{\mathrm{V}}\right]^{-1}\left\{\mathbf{g}^{\mathrm{V}}\right\}. \tag{8}$$

Substituting expressions (8) into (1), considering the arbitrariness of $\{\widetilde{\mathbf{g}}\}$ and the fact that in the case considered all matrices and $\left\{\mathbf{g}^{\mathrm{V}}\right\}$ do not depend on coordinates, calculating the definite integral in (1), for each finite element of a vertebra we obtain

$$\left\{\mathbf{R}^{\mathrm{V}}\right\} = \left[\mathbf{K}^{\mathrm{V}}\right]\left\{\mathbf{g}^{\mathrm{V}}\right\}, \tag{9}$$

where $\left[\mathbf{K}^{\mathrm{V}}\right] = V\left[\mathbf{D}^{\mathrm{V}}\right]^{\mathrm{T}}\left[\mathbf{E}_0\right]\left[\mathbf{D}^{\mathrm{V}}\right]$ is the stiffness matrix of the finite element of the vertebra, $\left[\mathbf{D}^{\mathrm{V}}\right] = \left[\mathbf{C}^{\mathrm{V}}\right]\left[\mathbf{B}^{\mathrm{V}}\right]^{1}$.

By performing the matrix operations in (9), we obtain

$$\left[\mathbf{K}^{\mathrm{V}}\right] = \frac{1}{36V}\begin{bmatrix} \mathbf{k}_{11} & \mathbf{k}_{12} & \mathbf{k}_{13} & \mathbf{k}_{14} \\ \mathbf{k}_{21} & \mathbf{k}_{22} & \mathbf{k}_{23} & \mathbf{k}_{24} \\ \mathbf{k}_{31} & \mathbf{k}_{32} & \mathbf{k}_{33} & \mathbf{k}_{34} \\ \mathbf{k}_{41} & \mathbf{k}_{42} & \mathbf{k}_{43} & \mathbf{k}_{44} \end{bmatrix},$$

where

$$\mathbf{k}_{ij}t = \begin{bmatrix} b_i b_j \rho + (c_i c_j + d_i d_j)G & b_i c_j \lambda + c_i b_j G & b_i d_j \lambda + d_i b_j G \\ c_i b_j \lambda + b_i c_j G & c_i c_j \rho + (b_i b_j + d_i d_j)G & c_i d_i \lambda + d_i c_j G \\ d_i b_j \lambda + b_i d_j G & d_i c_j \lambda + c_i d_j G & d_i d_j \rho + (c_i c_j + b_i b_j)G \end{bmatrix},$$

$$\rho = 2G + \lambda, \quad i = \overline{1, 4}, \; j = \overline{1, 4}.$$

3. Finite element model of the intervertebral disc

The ratio of the characteristic size of the intervertebral disc in plan to its thickness is between 10 and 100. Consequently, to determine the SSD of the disc, it is possible to use the theory of bending of thin plates based on the Kirchhoff–Love assumptions [Zienkiewicz, Taylor, 2000]:

1. The intervertebral disc does not experience any deformation in the medial plane. During bending, this plane remains neutral:
$$u_0 = \vartheta_0 = 0, \tag{10}$$
where u_0 and ϑ_0 are the displacements of points of the median plane along the X and Y axes.
2. The points of the disk lying on the normal to the median plane before loading remain on the normal to its median surface during the bending process:
$$\begin{cases} \gamma_{yz} = 0, \\ \gamma_{zx} = 0, \end{cases} \tag{11}$$
$$\varepsilon_z = 0. \tag{12}$$
3. The normal stresses in the direction transverse to the median plane of the disk can be neglected:
$$\sigma_z = 0. \tag{13}$$

During loading, the intervertebral disc deforms in a linear-elastic manner until the stress value is equal to a certain value. If the stresses continue to increase, the disc will exhibit nonlinear properties.

Next, we will consider only the loading process and consider the following hypotheses:

1. Volumetric deformation is elastic, i. e., due to nonlinear deformation, the volume of the body does not change:
$$\sigma_{av} = K\theta = 3K\varepsilon_{av}, \tag{14}$$
where σ_{av} is the average normal stress; θ is the volume deformation; ε_{av} is the average normal deformation; $K = \frac{E}{3(1-2v)}$ is the volumetric modulus of elasticity, E is the elastic modulus, v is Poisson's ratio, while $\sigma_{av} = \frac{\sigma_x+\sigma_y+\sigma_z}{3}$, $\varepsilon_{av} = \frac{\varepsilon_x+\varepsilon_y+\varepsilon_z}{3}$, $\theta = 3\varepsilon_{av}$, and σ_x, σ_y, σ_z are normal stresses.

2. Stress and strain deviators are identical up to a constant multiplier:
$$s_{ij} = \frac{2}{3}\frac{\sigma_{in}}{\varepsilon_{in}}e_{ij}, \tag{15}$$
where
$$\sigma_{in} = \frac{1}{\sqrt{2}}\sqrt{(\sigma_x-\sigma_y)^2+(\sigma_y-\sigma_z)^2+(\sigma_z-\sigma_x)^2+6\left(\tau_{xy}^2+\tau_{yz}^2+\tau_{zx}^2\right)}$$
is the stress intensity; s_{ij} are the stress deviator components; e_{ij} are the components of the strain deviator; τ_{xy}, τ_{yz}, τ_{zx} are the tangential stresses;
$$\varepsilon_{in} = \frac{\sqrt{2}}{3}\sqrt{(\varepsilon_x-\varepsilon_y)^2+\varepsilon_x^2+\varepsilon_y^2+\frac{3}{2}\gamma_{xy}^2}$$
is the intensity of deformations; ε_x, ε_y are the axial deformations; and γ_{xy} are the shear deformations.

3. The ratio
$$\sigma_{in} = \Phi(\varepsilon_{in}) \tag{16}$$
does not depend on the specific type of stress state.

4. Procedure for determining nonlinear deformations of the intervertebral disc

Suppose that there exists a linearly elastic homogeneous hypothetical intervertebral disc with the same shape and the same boundary conditions whose deformations under a given load coincide with those of the real disc. Then, by assuming the accepted hypotheses, we will have the equality of work of the hypothetical elastic disc and the real intervertebral disc. Then, according to the potential energy principle [Zienkiewicz, Taylor, 2000],
$$\delta_\varepsilon\Pi = \delta_\varepsilon(W - A) = 0,$$
where the symbol "δ_ε" indicates that only the deformations and displacements vary, Π is the potential energy of the intervertebral disc, $W = \int_V U\,dV$ is the work of deformation, A is the work of external forces, and U is the potential specific energy of deformation of the intervertebral disc, we will have:
$$\delta_\varepsilon\left(W^{\mathrm{L}} - W^{\mathrm{N}}\right) = \delta_\varepsilon\left(\int_V \left(U^{\mathrm{L}} - U^{\mathrm{N}}\right)dV\right) = 0, \tag{17}$$
where the superscript "L" refers to the linearly elastic disc, and the superscript "N" refers to the nonlinearly elastic disc, W^{L} is the work of deformations in a hypothetical linearly elastic disk, W^{N} is

the work of the deformations in the real intervertebral disc, $U^{L} = \int_{0}^{\varepsilon_{ij}} \sigma_{ij}^{L}\, d\varepsilon_{ij}$ is the specific potential deformation energy of a linearly elastic disk, $U^{N} = \int_{0}^{\varepsilon_{ij}} \sigma_{ij}^{N}\, d\varepsilon_{ij}$ is the specific deformation energy of the nonlinearly elastic intervertebral disc, and ε is the average normal deformation. Moreover, for a linearly elastic disk, according to (17), we can obtain:

$$U^{L} = \int_{0}^{\varepsilon_{ij}} \sigma_{ij}^{L}\, d\varepsilon_{ij} = \frac{\sigma_{in}^{L}\varepsilon_{in}}{2} + K\frac{\varepsilon^{2}}{2}. \tag{18}$$

According to the accepted hypotheses (14)–(16), we will have:

$$U^{N} = \int_{0}^{\varepsilon_{ij}} \sigma_{ij}^{N}\, d\varepsilon_{ij} = \int_{0}^{\varepsilon_{in}} \Phi(\varepsilon_{in})\, d\varepsilon_{in} + K\frac{\varepsilon^{2}}{2}, \tag{19}$$

where $\Phi(\varepsilon_{in})$ is the universal function.

Insert (18) and (19) into (17):

$$\delta_{\varepsilon}\left(\int_{V}\left(\frac{\sigma_{in}^{L}\varepsilon_{in}}{2} - \int_{0}^{\varepsilon_{in}} \Phi(\varepsilon_{in})\, d\varepsilon_{in}\right)dV\right) = \int_{V} \delta_{\varepsilon}\varepsilon_{in}\left(\frac{\sigma_{in}^{L}}{2} - \frac{1}{\varepsilon_{in}}\int_{0}^{\varepsilon_{in}} \Phi(\varepsilon_{in})\, d\varepsilon_{in}\right)dV = 0. \tag{20}$$

It follows from (20) that

$$\frac{\sigma_{in}^{L}}{2} = \frac{1}{\varepsilon_{in}}\int_{0}^{\varepsilon_{in}} \Phi(\varepsilon_{in})\, d\varepsilon_{in}.$$

From the last equation, by integrating with a given universal function $\Phi(\varepsilon_{in})$, it is possible to express

$$\sigma_{in}^{N} = \psi\left(\sigma_{in}^{L}\right). \tag{21}$$

Suppose that there exists a linearly elastic disc with elastic modulus E and Poisson's coefficient V of the same shape and dimensions, coinciding with the original real intervertebral disc and having the same boundary conditions, whose deformations under certain external loading conditions R^{*} will coincide with the deformations of the intervertebral disc under specified loads R.

Let us determine the loads. It is known [Gorshkov et al., 2002] that stresses depend only on the magnitude of the internal force acting on an elementary area as its dimensions tend to zero. In this case, relation (21) is valid for any elastic intervertebral disc having the same shape as the original nonlinearly elastic one. The boundary conditions for these two discs are identical.

Let us find the stresses σ_{in}^{*} in the hypothetical disc under loads R^{*}. Obviously, if the stresses in the nonlinearly elastic disc and ε_{in} are the corresponding strains, then the following relations hold:

$$\frac{\sigma_{in}^{*}}{\sigma_{in}^{N}} = \frac{\varepsilon_{in}}{\varepsilon_{in}^{L}},$$

where ε_{in}^{L} are deformations in the hypothetical disk corresponding to the stresses σ_{in}^{N}.

Then, according to the principle of virtual displacements [Zienkiewicz, Taylor, 2000] and the adopted hypotheses (11)–(13), relations (1) hold.

Assuming that the required displacements and strains are known, we express them from the relations for the linearly elastic disc and substitute them into the relations for the nonlinearly elastic disc.

Since for elastic bodies the strain rate changes in proportion to the stress rate, it is not difficult to express:

$$R^{*} = F\left(\sigma_{in}^{\mathrm{L}}, \varepsilon_{in}^{\mathrm{L}}, \psi\left(\sigma_{in}^{\mathrm{L}}\right), R, E, \nu\right). \tag{22}$$

Thus, determining nonlinear deformations of the intervertebral disc requires solving the elasticity problem twice. In the first case, the initial vector R is used; in the second case, the new vector R^{*} is used. At each pass, the stiffness matrix [Zienkiewicz, Taylor, 2000] remains unchanged, which significantly reduces the time required for repeatedly solving the system of linear algebraic equations.

5. Mathematical model of the functional spinal unit

All vertebrae are discretized using tetrahedral finite elements, and the intervertebral discs are discretized using planar quadrilateral finite elements. A conforming shared discretized interface is enforced between system components so that each finite element belongs entirely to one and only one component.

Using (9) and assuming that the direction of axis OZ coincides with the direction of vertical forces, we will have the following nodal displacements on the lower face (upper face) of the vertebra: $\left\{\mathbf{g}^{\mathrm{pl}}\right\} = [\mathbf{L}]\left\{\boldsymbol{g}_{\mathrm{av}}^{\mathrm{pl}}\right\}$,

$$[L] = \begin{bmatrix} [M] & [Z] & [Z] & [Z] \\ [Z] & [M] & [Z] & [Z] \\ [Z] & [Z] & [M] & [Z] \\ [Z] & [Z] & [Z] & [M] \end{bmatrix}, \quad [\mathbf{M}] = \begin{bmatrix} 0 & 0 & \frac{h}{2} \\ 0 & \frac{h}{2} & 0 \\ 1 & 0 & 0 \end{bmatrix}, \quad [\mathbf{z}] = \begin{bmatrix} 0 & 0 & 0 \\ 0 & 0 & 0 \\ 0 & 0 & 0 \end{bmatrix}.$$

Therefore,

$$\left\{\mathbf{g}_{\mathrm{av}}^{\mathrm{pl}}\right\} = \left[\mathbf{L}^{-1}\right]\left\{\mathbf{g}^{\mathrm{pl}}\right\}. \tag{23}$$

By substituting equality (23) into (1), we obtain the basic equation of the FEM in displacements for the lower plane of the vertebra:

$$\left\{\mathbf{R}^{\mathrm{pl}}\right\} + \left\{\mathbf{R}_{\mathrm{nf}}^{\mathrm{pl}}\right\}_{i+1} = \left[\mathbf{K}^{\mathrm{pl}}\right]_{i+1}\left[\mathbf{L}^{-1}\right]\left\{\mathbf{g}^{\mathrm{pl}}\right\}_{i+1}. \tag{24}$$

The stiffness matrix of the whole system is constructed in the following order:

$$K_{ij}^{\mathrm{gl}} = \sum_{r=1}^{N} K_{ij}^{r},$$

where N is the number of finite elements with which the system under consideration is discretized; K_{ij}^{gl} is the element of the global stiffness matrix $\left\lfloor\mathbf{K}^{\mathrm{gl}}\right\rfloor$, characterizing the contribution of the j-th unit displacement to the i-th component of the nodal forces of the system as a whole; K_{ij}^{r} is the stiffness matrix element $\lfloor\mathbf{K}^{r}\rfloor$ r-th finite element, characterizing the contribution of the j-th unit displacement to the i-th component of the nodal forces, and the stiffness matrices $[\mathbf{K}^{r}]$ can be calculated by formulas similar to (9).

Of course, under the sign of the sum, only the elements adjacent to the node where the i-th force component is applied will give a nonzero contribution. Thus, for the whole system under consideration:

$$\left[\mathbf{K}^{\mathrm{gl}}\right]\left\{\mathbf{g}^{\mathrm{nod}}\right\} = \{\mathbf{R}\} + \{\mathbf{R}_{\mathrm{nf}}\}, \tag{25}$$

where $\left[\mathbf{K}^{\mathrm{gl}}\right]$ is the global stiffness matrix; $\left\{\mathbf{g}^{\mathrm{nod}}\right\}$ is the vector of node displacements of the whole system; $\{\mathbf{R}\}$ is the nodal force vector; $\{\mathbf{R}_{\mathrm{nf}}\}$ is the vector of nodal forces, defined for the finite elements of the vertebrae.

The resulting governing finite element equation (24) for determining the SSD of the system is solved subject to boundary conditions. To determine nonlinear deformations, system (25) is solved twice. First, the linear solution is obtained; then, for intervertebral disc elements where the computed strain values exceed the limiting values, additional forces are determined, and system (25) is solved again with a new nodal force vector.

6. Verification of the numerical solution

According to medical terminology, the lumbar spine consists of five vertebrae labeled L1–L5 and four intervertebral discs. A simplified diagram of the problem in question is shown in Fig. 2.

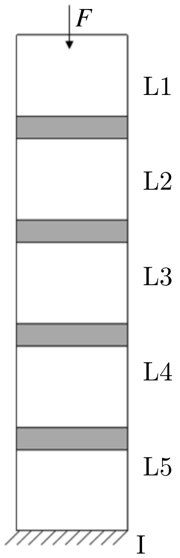

Figure 2. Computational scheme of the problem

Figure 2 shows the vertebrae in white color and the intervertebral discs in gray. Above the five vertebrae of the lumbar spine are 19 vertebrae of the cervical and thoracic spine. The load of $F = 1000N$ was applied to the lumbar first vertebra (upper boundary) of the L1 lumbar spine. The basal plate (lower border) of the L5 vertebra was fixed stationary (no movement along the three coordinate axes).

Two variants of geometric primitives were used to construct a simplified geometric model of the lumbar spine:

1) parallelepipeds;

2) cylinders.

The model is represented as a set of primitives of different heights, equal to the average height of elements of the lumbar spine of an adult person in the usual state. Primitives simulating vertebrae have a height of 28.9 mm, and primitives simulating intervertebral discs have a height of 8.1 mm [Zienkiewicz, Taylor, 2000; Hurtado-Aviles et al., 2021]. The total height of the geometric model is 176.9 mm.

In order to obtain the same spinal deformation energy, the simplified and real geometric models should consist of elements of the same volumes, i. e., if the heights of elements are equal, the cross-sectional areas of bases should be equal, and take the value of 1375 mm^2 [Ablyazov et al., 2014].

Due to the same area and shape of the base, the spine elements are in contact throughout the base, which simplifies load transfer between the vertebral elements, while ensuring the continuity of stress and strain values near the vertebral-intervertebral disc boundary.

The optimal step of the finite-element mesh was determined using simplified models of the lumbar spine. Each element of the geometric model was divided by horizontal planes into several layers, each layer was divided into parallelepipeds similar in shape to a cube, each parallelepiped — into 5 tetrahedrons. When the layers are partitioned into parallelepipeds, the nodes of the finite element mesh at the vertebrae-disk boundary coincide. The sizes of finite elements of vertebrae and intervertebral discs differed by no more than 10 %. As a result of successive doubling of intervertebral disc finite element layers and commensal increase in vertebral layers, the maximum size of the tetrahedron edge equal to 1.95 mm was determined. The increase in equivalent stress compared to the last iteration was 2.48 %.

The resulting larger finite element size was used to develop a 3D model of the lumbar spine of a real patient, generate a finite element mesh, and determine the SSD of the lumbar spine using the Comsol package. This was done using a 3D model constructed from a series of CT images of the spine of a real patient (Fig. 3). The boundary conditions and rheological models were the same as for the simplified spine models.

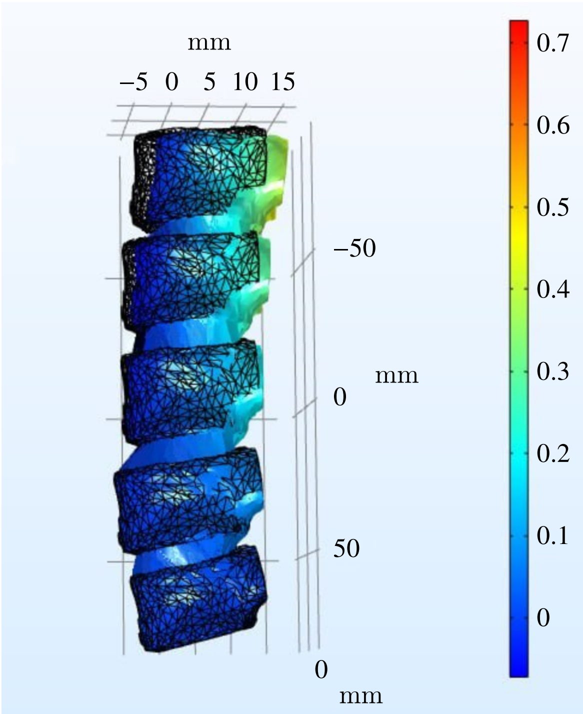

Figure 3. 3D model and SSD of the patient’s spine

In Fig. 4, longitudinal deformation values are presented for points located on the vertical axis of the lumbar spine. The origin of this axis is at the load application point (the endplate of vertebra L1).

The figure shows that each curve has a section from 150 to 176.9 mm with a significant increase in deformations. Such a character of deformations is caused by the influence of stress concentration in the neighborhood of the acting concentrated load. Therefore, this section is excluded from consideration.

The curve corresponding to the linear deformation behavior of the parallelepipeds differs substantially; except for the above-mentioned segment, it remains linear. The other curves include near-linear segments in regions of linearly elastic deformation of the vertebrae and nonlinear segments caused by nonlinear deformation of the intervertebral discs.

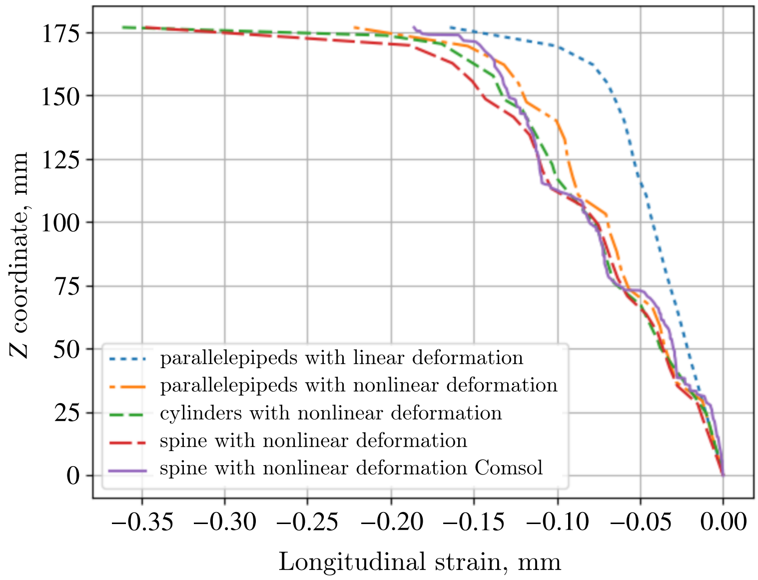

Figure 4. Simulation results

The discrepancy between the values of longitudinal deformation values of the numerical solution according to the proposed mathematical model and the solution obtained using Comsol is 10 %.

Conclusions

The use of volumetric figures of simple shape to describe the geometry of vertebrae and intervertebral discs simplifies the algorithm for obtaining a finite-element mesh, which significantly affects the quality of the finite-element model by using finite elements of classical shape without significant distortions. It also improves the quality of the obtained results due to a fairly simple process of changing the density of the mesh when investigating the convergence of the results obtained, as well as comparing the averaged values in the neighboring finite elements.

Accounting for nonlinear deformations of the intervertebral discs significantly changed both the pattern and the magnitude of deformation of the human lumbar spine.

The resulting accurate anthropometric finite element model allows us to determine the stress-strain state of the human lumbar spine for the purpose of predicting the development of musculoskeletal disorders.

The proposed approach for intervertebral discs nonlinear deformations yielded results that are accurate enough for practical applications compared to the Comsol solution.

References

Ablyazov O. V., Khudoiberdiev K. T., Kondratiev A. V., Ablyazov A. A. MRI-spondylometry in the assessment of normal anatomical values of the lumbar segment of the spine // Bulletin of Emergency Medicine. — 2014. — No. 4. — P. 54–56.

Anisimova E. A., Emkuzhev O. L., Anisimov D. I., Popryga D. V., Lukina G. A., Yakovlev N. M. Comparative analysis of morphological and topometric parameters of lumbar spine in normal state and in degenerative-dystrophic changes // Saratov Journal of Medical Scientific Research. — 2015. — Vol. 11, No. 4. — P. 515–520.

Barysh A. E., Buznitsky R. I., Jaresko A. V. Mathematical modeling of vertebral motor segments CIII-CVII by the finite element method // Injury. — 2012. — No. 13. — P. 248–253.

Best B. A., Guilak F., Setton L. A., Zhu W., Saed-Nejad F., Ratcliffe A., Weidenbaum M., Mow V. C. Compressive mechanical properties of the human annulus fibrosus and their relationship to biochemical composition // Spine. — 1999. — No. 19. — P. 212–221.

Bublik L. A., Likholetov A. N. Experimental biomechanical substantiation of transpedicular fusion with vertebroplasty based on the study of a finite element model of a spinal column fragment // Trauma. — 2014. — No. 15. — P. 123–133.

Bublik L. A., Likholetov A. N., Beigelzimer Ya. E., Kulagin R. Yu. Study of the stress-strain distribution of a finite element model of a fragment of the spinal column with the combined use of transpendicular implants and vertebroplasty // Neurosurgery and Neurology of Kazakhstan. — 2013. — No. 3 (32). — P. 3–7.

Cansel S. D. Nonlinear finite element analysis of intervertebral disc: a comparative study // Sakarya university journal of science. — 2018. — No. 5. — P. 1–7.

Chou A. I., Bansal A., Miller G. J., Nicoll S. B. The effect of serial monolayer passing on the collagen expression profile of outer and inner anulus fibrosus cells // Spine. — 2006. — No. 17. — P. 1875–1881.

Coogan J. S, Francis W. L., Eliason T. D., Bredbenner T. L., Stemper B. D., Yoganandan N., Pintar F. A., Nicolella D. P. Finite element of a lumbar intervertebral disc nucleus replacement device // Frontiers in Bioengineering and Biotechnology. — 2016. — No. 3. — P. 1–11.

Eremin A. V., Luzin V. I., Zakharov A. A., Fomina K. A., Fastova O. N. Modeling the behavior of the human lumbosacral joint depending on the morphotype of the sacrum // Bulletin of the VSNC SO RAMS. — 2011. — No. 4. — P. 246–248.

Furlong D. R., Palazotto A. N. A finite element analysis of the influence of surgical herniation on the viscoelastic properties of the intervertebral disc // J. Biomech. — 1983. — No. 16. — P. 785–795.

Gorshkov A. G., Starovoitov E. I., Tarlakovsky D. V. Theory of elasticity and plasticity. — Fizmatlit, 2002. — 416 p.

Goto K., Tajima N., Chosa E., Totoribe K., Kuroki H., Arizumi Y., Arai T. Mechanical analysis of lumbar vertebrae in three-dimensional finite element model in which intradiscal pressure 464 spine technology handbook in the nucleus pulposus was used to establish the model // J. Orthop. sci. — 2002. — Vol. 7. — P. 243–246.

Hurtado-Aviles J., Roca-González J., Kurachka K. S. Developing of a mathematical model to perform measurements of axial vertebral rotation on computer-aided and automated diagnosis systems, using Raimondi's method // Radiology Research and Practice. — 2021. — Vol. 2021. — P. 1–9.

Joshi A., Massey C. J., Karduna A., Vresilovic E., Marcolongo M. The effect of nucleus implant parameters on the compressive mechanics of the lumbar intervertebral disc: a finite element study // J. Biomed. mater. Res. BAppl. biomater. — 2009. — Vol. 90B, No. 2. — P. 596–607.

Korzh N. A., Barysh A. E., Buzinitsky R. I., Yeresko A. V. Mathematical modeling of anterior interbody cervicospondylodesis with vertical cylindrical mesh implants // Orthopedics, Traumatology and Prosthetics. — 2012. — No. 4. — P. 5–12.

Korzh T. A., Staude V. A., Kondratiev A. V., Karpinsky M. Yu. Stress-strain distribution of the kinematic chain "lumbar spine-sacrum-pelvis" with asymmetry of the joint spaces of the sacroiliac joint // Orthopedics, traumatology and prosthetics. — 2015. — No. 3. — P. 5–10.

Kurachka K. S., Tsalka I. M. Vertebrae detection in X-ray images based on deep convolutional neural networks // 2017 IEEE 14th International Scientific Conference on Informatics, 14–16 Nov. 2017. — 2017. — P. 194–196.

Kurochka K. S. Construction of a mathematical model of a complex system of inhomogeneous viscoelastic dispersed and solid solids // Structural mechanics of engineering structures and structures. — 2007. — No. 4. — P. 18–31.

Kurochka K. S, Panarin K. A. Algorithm of definition of mutual arrangement of L1–L5 vertebrae on X-ray images // Optical Memory and Neural Networks. — 2018. — Vol. 27. — P. 161–169.

Meakin J. R. Replacing the nucleus pulposus of the intervertebral disk: prediction of suitable properties of a replacement material using finite element analysis // J. mater. sci. mater. Med. — 2001. — No. 12. — P. 207–213.

Mezentsev A. A., Petrenko D. E., Barkov A. A., Yaresko A. V. Study of the stress-strain distribution of the "implant-lumbar spine-pelvis" system with different fixation options // Orthopedics, traumatology and prosthetics. — 2011. — No. 2. — P. 37–41.

Nagy G. T., Gentle C. R. Significanse of the annulus properties to finite element modeling of intervertebral discs // Journal of Musculoskeletal Research. — 2001. — No. 4. — P. 159–171.

Obraztsov I. F. Strength problems in biomechanics. — Moscow: Higher School, 1988. — 311 p.

Orlov S. V. Mathematical modeling of spinal injury // Bulletin of the Baltic Federal University. I. Kant. — 2011. — No. 10. — P. 47–55.

Palatinskaya I. P., Dolganina N. Yu., Poptsova T. Yu. Supercomputer modeling of dynamic loads of the lumbar spine // Bulletin of the USATU. — 2012. — Vol. 17, No. 5 (58). — P. 230–236.

Staude V. A., Kondratiev A. V., Karpinsky M. Yu. Numerical modeling and analysis of the stress-strain distribution of the sacroiliac joint in various variants of lumbar lordosis // Orthopedics, traumatology and prosthetics. — 2012. — No. 2. — P. 50–56.

Strack D., Mesbah M., Kirschke J. Interpatient variability and validation of simplified L4–L5 Finite Element Model //XXX Congress of the International Society of Biomechanics. — 2025. — P. 10.

Strange D. G., Fisher S. T., Boughton P. C., Kishen T. J., Diwan A. D. Restoration of compressive loading properties of lumbar discs with a nucleus implant — a finite element analysis study // Spine J. — 2010. — No. 10. — P. 602–609.

Tsurova N. Kh. Biomechanical modeling and study of the segment of the lumbar spine // Biotechnical systems in medicine and ecology. — 2011. — No. 4. — P. 73–78.

Veretelnik O. V., Tkachuk N. A., Timchenko I. B., Dynnik A. A., Burnt A. V. Mathematical and numerical study of various designs of orthoses for spondylodesis of the cervical spine // Bulletin of NTU KhPI. — 2014. — No. 29 (1072). — P. 27–37.

Yang H., Jekir M. J., Davis M. W., Keaveny T. M. Effective modulus of the human intervertebral disc and its effect on vertebral bone stress // J. Biomech. — 2016. — Vol. 49, No. 7. — P. 1134–1140.

Zander T., Rohlmann A., Calisse J. Estimation of muscle forces in the lumbar spine during upper-body inclination // Clin. Biomech. — 2001. — No. 16. — P. 573–580.

Zharnov A. M., Zharnova O. A. Biomechanical processes in the vertebral motor segment of the cervical spine during its movement // Russian Journal of Biomechanics. — 2014. — Vol. 18, No. 2. — P. 105–118.

Zienkiewicz O. C., Taylor R. L. The finite element method. Vol. 1: The basics. — Fifth edition. — Butterworth-Heinemann, 2000. — 689 p.

Zienkiewicz O. C., Taylor R. L. The finite element method. Vol. 2: Solid mechanics. — Fifth edition. — Butterworth-Heinemann, 2000. — 459 p.

Zinnatova N. Kh. Biomechanical method for diagnosing the state of the spine in normal and pathological conditions // Izvestiya SFedU. Technical science. — 2009. — P. 109–113.